

Design and analysis of grid connected photovoltaic system for Step-up Resonant Converter

Esenipalli Anil

M-tech Student Scholar Department of Electrical & Electronics Engineering, Avanathi Institute of Engineering and Technology, Vizianagaram (Dist.), A.P, India.

A Arjuna Rao

Associate Professor Department of Electrical & Electronics Engineering, Avanathi Institute of Engineering and Technology, Vizianagaram (Dist.), A.P, India.

Abstract—In the grid connected photovoltaic system for Step-up Resonant Converter, processes of multiple dc-ac-dc or ac-dc-ac conversions are reduced in an individual ac or dc grid. The grid consists of ac and connected together by multi directional converters. In this micro grid network, it is especially difficult to support the critical load without incessant power supply. The generated power can be extracted under varying wind speed, solar irradiation level and can be stored in batteries at low power demands. In this paper, AC-DC micro grid with solar energy, energy storage, and a pulse load is proposed. This micro grid can be viewed as a PEV parking garage power system or a ship's power system that utilizes sustainable energy and is influenced by a pulse load. The battery banks inject or absorb energy on the DC bus to regulate the DC side voltage. The frequency and voltage of the AC side are regulated by a bidirectional AC-DC inverter. The power flow control of these devices serves to increase the system's stability and robustness. The system is simulated in Matlab/Simulink.

Index Terms—Renewable energy, resonant converter, soft switching, voltage step-up, voltage stress.

I. INTRODUCTION

In general, manufacturers provide 5 second and ½ an hour surge figures which give an indication of how much power is supplied by the inverter. Solar inverters require a high efficiency rating. Since use of solar cells remains relatively costly, it is paramount to adopt high efficiency inverter to optimize the performance of solar energy system. High reliability helps keep maintenance cost low. Since most solar power stations are built in rural areas without any monitoring manpower, it requires that inverters have competent circuit structure, strict

selection of components and protective functions such as internal short circuit protection, overheating protection and overcharge protection. Wider tolerance to DC input current plays an important role, since the terminal voltage varies depending on the load and sunlight [1-4]. Though energy storage batteries are significant in providing consistent power supply, variation in voltage increases as the battery's remaining capacity and internal resistance condition changes especially when the battery is ageing, widening its terminal voltage variation range. In mid-to-large capacity solar energy systems, inverters' power output should be in the form of sine waves which attain less distortion in energy transmission. Many solar energy power stations are equipped with gadgets that require higher quality of electricity grid, when connected to the solar systems, requires sine waves to avoid electric harmonic pollution from the public power supply.[5] How Inverters Work: There are three major functions an inverter provides to ensure the operation of a solar system One of the most efficient and promising way to solve this problem is the use of pumping and water treatment systems supplied by photovoltaic (PV) solar energy. Such systems aren't new, and are already used for more than three decades [6-8].

But until recently the majority of the available commercial converters are based on an intermediate storage system performed with the use of batteries or DC motors to drive the water pump. The batteries allow the system to always operate at its rated power even in temporary conditions of low solar radiation [9-10]. This facilitates the coupling of the electric dynamics of the solar panel and the motor used for pumping. Generally, batteries used in this type of system have a low life span, only two years on average, which is extremely low compared to useful life of 15 years of a photovoltaic module. Also, they

make the cost of installation and maintenance of such systems substantially high.

These systems are directly coupled to the electric distribution network and do not require battery storage. Figure.1 describes the basic system configuration. Electric energy is either sold or bought from the local electric utility depending on the local energy load patterns and the solar resource variation during the day, this operation mode requires an inverter to convert DC currents to AC currents. There are many benefits that could be obtained from using grid-tied PV systems instead of the traditional stand-alone schemes [11-12]. The benefits are:

- Smaller PV arrays can supply the same load reliably.
- Less balance of system components are needed.
- Comparable emission reduction potential taking advantage of existing infrastructure.
- Eliminates the need for energy storage and the costs associated to substituting and recycling batteries for individual clients. Storage can be included if desired to enhance reliability for the client.
- Takes advantage of the existing electrical infrastructure.
- Efficient use of available energy. Contributes to the required electrical grid generation while the client's demand is below PV output.

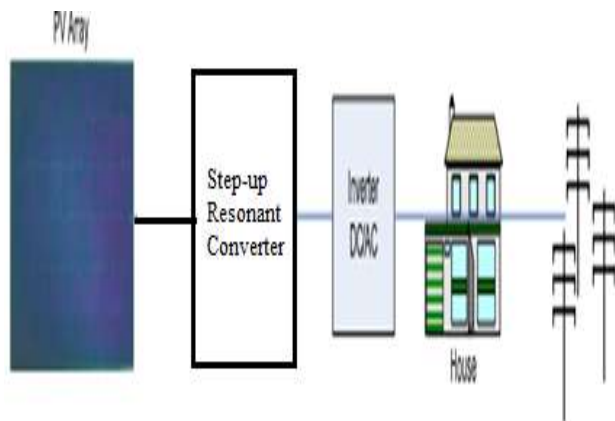


Fig.1.Grid-Tied Photovoltaic System.

Hybrid systems may be possible were battery storage or a generator (or both) can be combined with a grid connection for additional reliability and scheduling flexibility (at additional cost). [13] Most of the installed residential, commercial and central scale systems use pre-fabricated flat plate solar modules, because they are

widely available. Most 5-7 available reports on PV system costs are therefore related to this kind of technology and shall be our focus in this chapter. Other specialized technologies are available (e.g., concentrating PV systems), but not as commercially available as the traditional PV module.

II. CONVERTER STRUCTURE AND OPERATION PRINCIPLE

The proposed resonant step-up converter is shown in Fig. 2.

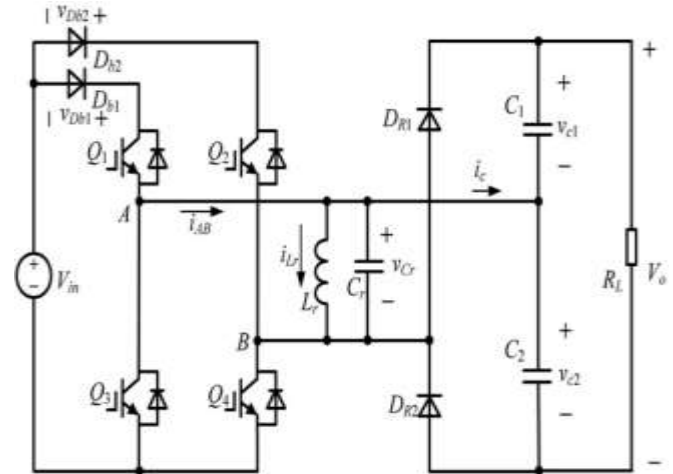


Fig. 2. Topology of the proposed resonant step-up converter.

The converter is composed of an FB switch network, which comprises Q_1 through Q_4 , an LC parallel resonant tank, a voltage doubler rectifier, and two input blocking diodes, $Db1$ and $Db2$.

The steady-state operating waveforms are shown in Fig. 3 and detailed operation modes of the proposed converter are shown in Fig. 4. For the proposed converter, Q_2 and Q_3 are tuned on and off simultaneously; Q_1 and Q_4 are tuned on and off simultaneously. In order to simplify the analysis of the converter, the following assumptions are made:

- 1) All switches, diodes, inductor, and capacitor are ideal components;
- 2) Output filter capacitors C_1 and C_2 are equal and large enough so that the output voltage V_o is considered constant in a switching period T_s .

A. Mode 1 [t_0, t_1] [See Fig. 4(a)]

During this mode, Q_1 and Q_4 are turned on resulting in the positive input voltage V_{in} across the LC parallel resonant tank, i.e., $V_{Lr} = V_{Cr} = V_{in}$. The converter operates similar to a conventional boost converter and the resonant inductor L_r acts as the boost inductor with the current through it increasing linearly from I_0 . The load is powered by C_1 and C_2 . At t_1 , the resonant inductor current i_{Lr} reaches I_1

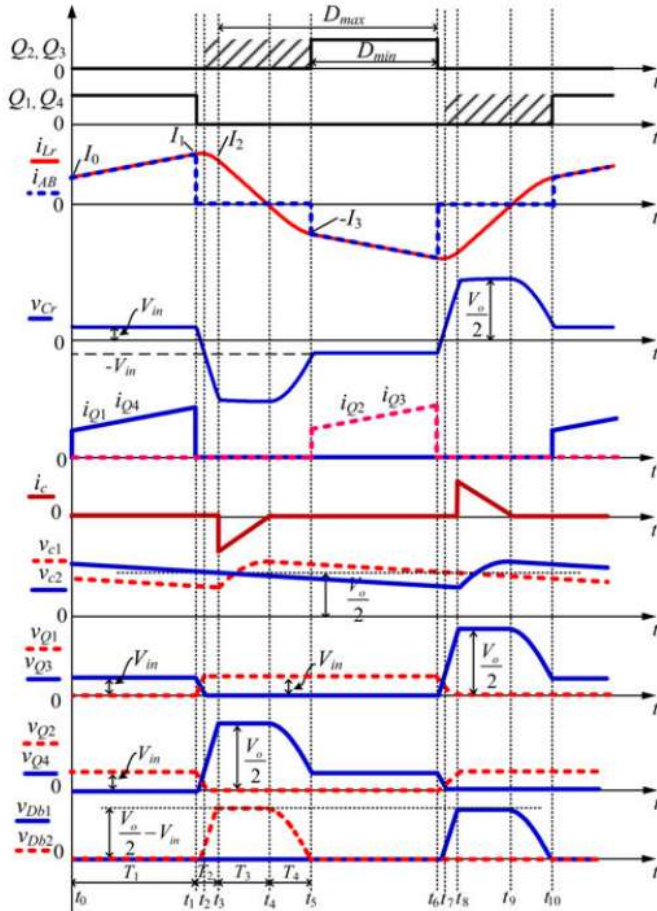


Fig. 3. Operating waveforms of the proposed converter.

$$I_1 = I_0 + \frac{V_{in} T_1}{L_r} \quad (1)$$

Where T_1 is the time interval of t_0 to t_1 .

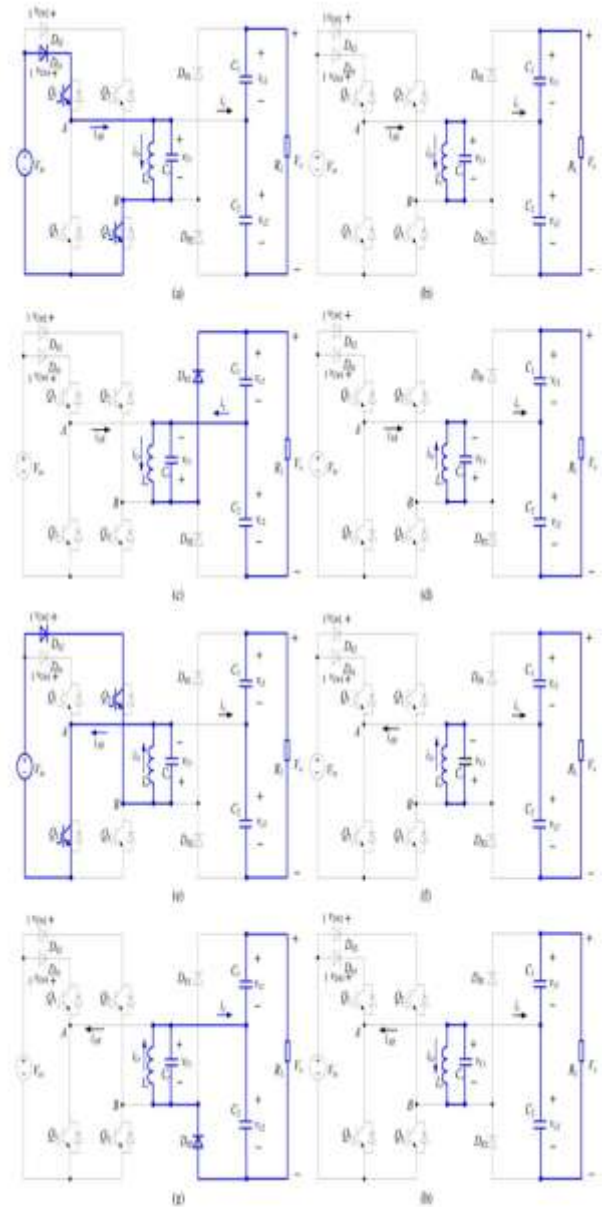


Fig. 4. Equivalent circuits of each operation stages. (a) $[t_0, t_1]$. (b) $[t_1, t_3]$. (c) $[t_3, t_4]$. (d) $[t_4, t_5]$. (e) $[t_5, t_6]$. (f) $[t_6, t_8]$. (g) $[t_8, t_9]$. (h) $[t_9, t_{10}]$.

In this mode, the energy delivered from V_{in} to L_r is

$$E_{in} = \frac{1}{2} L_r (I_1^2 - I_0^2) \quad (2)$$

B. Mode 2 $[t_1, t_3]$ [See Fig. 4(b)]

At t_1 , Q_1 and Q_4 are turned off and after that L_r resonates with C_r , V_{Cr} decreases from V_{in} , and i_{Lr} increases from I_0 in resonant form. Taking into account the parasitic output

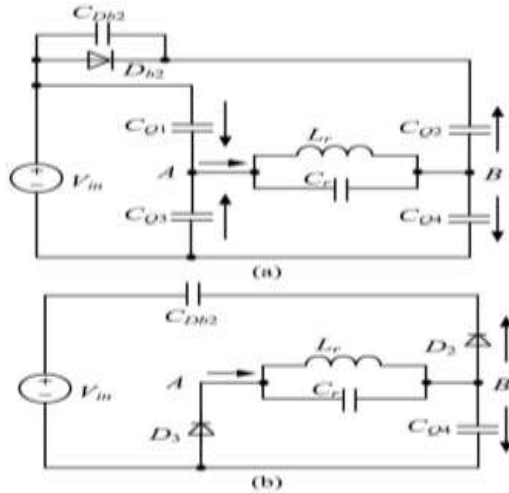


Fig. 5. Further equivalent circuits of Mode 2. (a) [t_1, t_2]. (b) [t_2, t_3].

Capacitors of Q_1 through Q_4 and junction capacitor of Db_2 , the equivalent circuit of the converter after t_1 is shown in Fig. 5(a), in which C_{Db_2} , C_{Q_1} , and C_{Q_4} are charged, C_{Q_2} and C_{Q_3} are discharged. In order to realize zero-voltage switching (ZVS) for Q_2 and Q_3 , an additional capacitor, whose magnitude is about ten times with respect to C_{Q_2} , is connected in parallel with Db_2 . Hence, the voltage across Db_2 is considered unchanged during the charging/discharging process and Db_2 is equivalent to be shorted. Due to C_r is much larger than the parasitic capacitances, the voltages across Q_1 and Q_4 increase slowly.

As a result, Q_1 and Q_4 are turned off at almost zero voltage in this mode. When V_{Cr} drops to zero, i_{Lr} reaches its maximum magnitude. After that, V_{Cr} increases in negative direction and i_{Lr} declines in resonant form. At t_2 , $V_{Cr} = -V_{in}$, the voltages across Q_1 and Q_4 reach V_{in} , the voltages across Q_2 and Q_3 fall to zero and the two switches can be turned on under zero-voltage condition. It should be noted that although Q_2 and Q_3 could be turned on after t_2 , there are no currents flowing through them. After t_2 , L_r continues to resonate with C_r , V_{Cr} increases in negative direction from $-V_{in}$, i_{Lr} declines in resonant form. Db_2 will hold reversed-bias voltage and the voltage across Q_4 continues to increase from V_{in} . The voltage across Q_1 is kept at V_{in} . The equivalent circuit of the converter after t_2 is shown in Fig. 5(b), in which D_2 and D_3 are the antiparallel diodes of Q_2 and Q_3 , respectively. This mode runs until V_{Cr} increases to $-V_o/2$ and i_{Lr} reduces to I_2 , at t_3 , the voltage across Q_4 reaches $V_o/2$ and the voltage across Db_2 reaches $V_o/2 - V_{in}$. It can be seen that during t_1 to t_3 , no power is transferred from the input source or to the load, and the whole energy stored in the LC resonant tank is unchanged, i.e.,

$$\frac{1}{2}L_r I_1^2 + \frac{1}{2}C_r V_{in}^2 = \frac{1}{2}L_r I_2^2 + \frac{1}{2}C_r \left(\frac{V_o}{2}\right)^2 \quad (3)$$

We have

$$i_{Lr}(t) = \frac{V_{in}}{Z_r} \sin[\omega_r(t-t_1)] + I_1 \cos[\omega_r(t-t_1)] \quad (4)$$

$$v_{Cr}(t) = V_{in} \cos[\omega_r(t-t_1)] - I_1 Z_r \sin[\omega_r(t-t_1)] \quad (5)$$

$$T_2 = \frac{1}{\omega_r} \left[\arcsin \left(\frac{V_{in}}{\sqrt{V_{in}^2 + \frac{L_r I_1^2}{C_r}}} \right) + \arcsin \left(\frac{V_o}{2\sqrt{V_{in}^2 + \frac{L_r I_1^2}{C_r}}} \right) \right] \quad (6)$$

Where $\omega_r = 1/\sqrt{L_r C_r}$, $Z_r = \sqrt{L_r/C_r}$, and T_2 is the time interval of t_1 to t_3 .

C. Mode 3 [t_3, t_4] [See Fig. 4(c)]

At t_3 , $V_{Cr} = -V_o/2$, DR_1 conducts naturally, C_1 is charged by i_{Lr} through DR_1 , V_{Cr} keeps unchanged, and i_{Lr} decreases linearly. At t_4 , $i_{Lr} = 0$. The time interval of t_3 to t_4 is

$$T_3 = \frac{2I_2 L_r}{V_o} \quad (7)$$

The energy delivered to load side in this mode is

$$E_{out} = \frac{V_o I_2 T_3}{4} \quad (8)$$

The energy consumed by the load in half-switching period is

$$E_R = \frac{V_o I_o T_s}{2} \quad (9)$$

Assuming 100% conversion efficiency of the converter and according to the energy conservation rule, in half-switching period

$$E_{in} = E_{out} = E_R \quad (10)$$

Combining (7), (8), (9), and (10), we have

$$I_2 = V_o \sqrt{\frac{I_o T_s}{V_o L_r}} \quad (11)$$

$$T_3 = 2\sqrt{\frac{T_s I_o L_r}{V_o}} \quad (12)$$

D. Mode 4 [t_4, t_5] [See Fig. 4(d)]

At t_4 , i_{Lr} decreases to zero and the current flowing through DR_1 also decreases to zero, and DR_1 is turned off with

zero current switching (ZCS), therefore, there is no reverse recovery. After t_4 , L_r resonates with C_r , C_r is discharged through L_r , V_{Cr} increases from $-V_o/2$ in positive direction, and i_{Lr} increases from zero in negative direction. Meanwhile, the voltage across Q_4 declines from $V_o/2$. At t_5 , $V_{Cr} = -V_{in}$, and $i_{Lr} = -I_3$. In this mode, the whole energy stored in the LC resonant tank is unchanged, i.e., where T_4 is the time interval of t_4 to t_5 .

$$\frac{1}{2}C_r \left(\frac{V_o}{2}\right)^2 = \frac{1}{2}L_r I_3^2 + \frac{1}{2}C_r V_{in}^2 \quad (13)$$

We have

$$I_0 = I_3 = \frac{1}{2} \sqrt{\frac{C_r(V_o^2 - 4V_{in}^2)}{L_r}} \quad (14)$$

$$i_{Lr}(t) = -\frac{V_o}{2\omega_r L_r} \sin[\omega_r(t - t_5)] \quad (15)$$

$$v_{Cr}(t) = \frac{-V_o \cos[\omega_r(t - t_5)]}{2} \quad (16)$$

$$T_4 = \frac{1}{\omega_r} \arccos\left(\frac{2V_{in}}{V_o}\right) \quad (17)$$

E. Mode 5 [t_5, t_6] [See Fig. 4(e)]

If Q_2 and Q_3 are turned on before t_5 , then after t_5 , L_r is charged by V_{in} through Q_2 and Q_3 , i_{Lr} increases in negative direction, and the mode is similar to Mode 1. If Q_2 and Q_3 are not turned on before t_5 , then after t_5 , L_r will resonate with C_r , the voltage of node A VA will increase from zero and the voltage of node B VB will decay from V_{in} , zero-voltage condition will be lost if Q_2 and Q_3 are turned on at the moment. Therefore, Q_2 and Q_3 must be turned on before t_5 to reduce switching loss. The operation modes during $[t_6, t_{10}]$ are similar to Modes 2–4, and the detailed equivalent circuits are shown in Fig. 4(f)–(h). During $[t_6, t_{10}]$, Q_2 and Q_3 are turned off at almost zero voltage, Q_1 and Q_4 are turned on with ZVS, and DR2 is turned off with ZCS.

III. A PHOTOVOLTAIC SYSTEM

The photovoltaic system converts sunlight directly to electricity without having any disastrous effect on our environment. The basic segment of PV array is PV cell, which is just a simple p-n junction device. The fig.6 manifests the equivalent circuit of PV cell. Equivalent circuit has a current source (photocurrent), a diode parallel to it, a resistor in series describing an internal resistance to the flow of current and a shunt resistance which expresses a leakage current. The current supplied to the load can be given as.

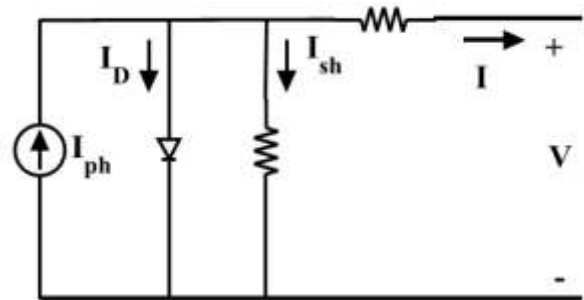


Fig 6 Equivalent circuit of Single diode model of a solar cell

$$I = I_{PV} - I_0 \left[\exp\left(\frac{V + IR_s}{aV_T}\right) - 1 \right] - \left(\frac{V + IR_s}{R_p}\right)$$

Where

I_{PV} –Photo current,

I_0 –diode's Reverse saturation current,

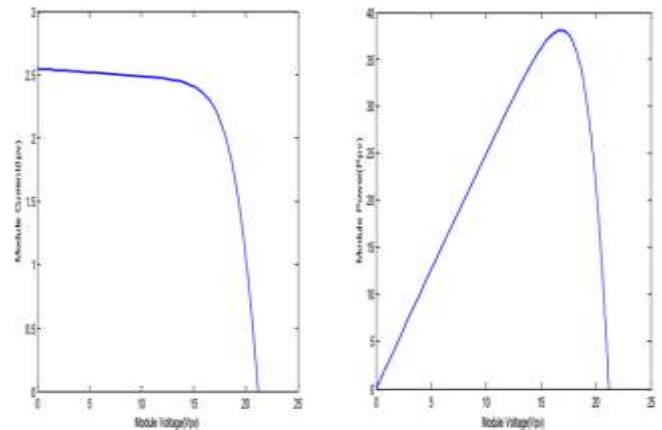
V –Voltage across the diode,

a – Ideality factor

V_T –Thermal voltage

R_s – Series resistance

R_p –Shunt resistance



This paper presents a single-phase inverter topology for grid-connected PV systems with a novel pulse width-modulated (PWM) control scheme. Two reference signals identical to each other with an offset equivalent to the amplitude of the triangular carrier signal were used to generate PWM signals for the switches. A digital proportional-integral current control to keep the current injected into the grid sinusoidal and to have high dynamic performance with rapidly changing atmospheric conditions. The proposed system is verified through simulation.

IV. MATLAB/SIMULATION RESULTS

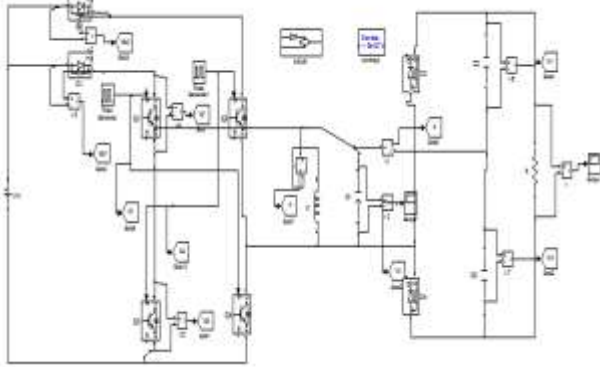


Fig.7. Matlab/Simulation circuit of the proposed resonant step-up converter.

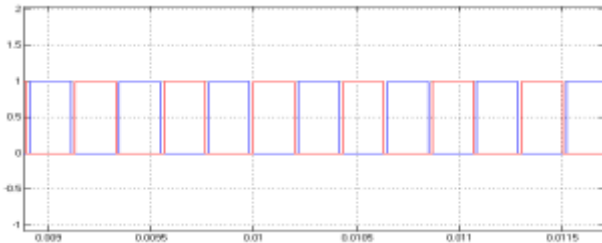


Fig.8. Simulation waveform of the switching pulses (Q_1 , Q_2 , Q_3 and Q_4) for 5MW.

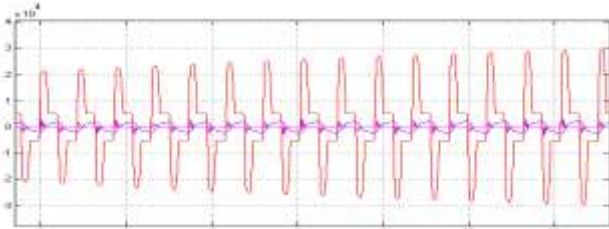


Fig.9. simulation waveform of resonant inductor current i_{Lr} , capacitor voltage V_{Cr} and capacitor Current i_c for 5MW.

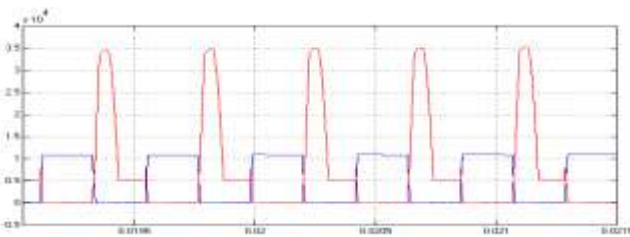


Fig.10. Simulation waveform of the switch voltages (V_{Q1} and V_{Q2}) for 5MW.

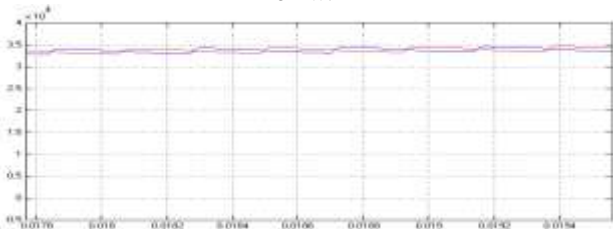


Fig.11. Simulation waveform of the output filter Capacitor Voltages (V_{C1} and V_{C2}) for 5 MW.

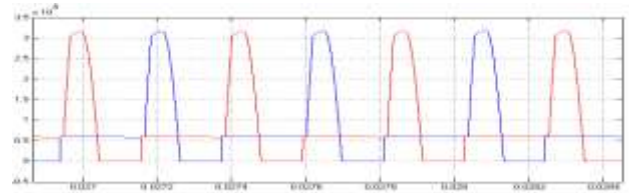


Fig.12. Simulation waveform of the input blocking diodes Voltages (V_{Db1} and V_{Db2}) for 5MW.

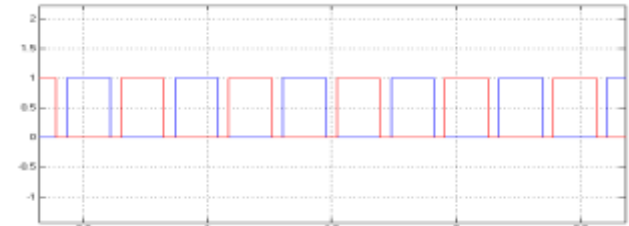


Fig.13. Simulation waveform of the switching pulses (Q_1 , Q_2 , Q_3 and Q_4) for 1MW.

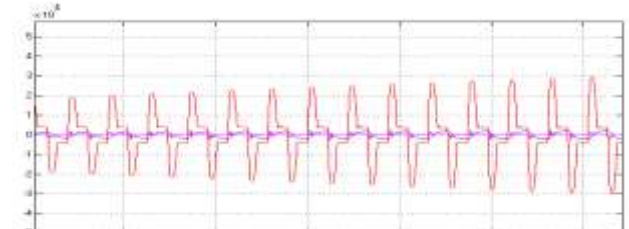


Fig.14. simulation waveform of resonant inductor current i_{Lr} , capacitor voltage V_{Cr} and capacitor Current i_c for 1MW.

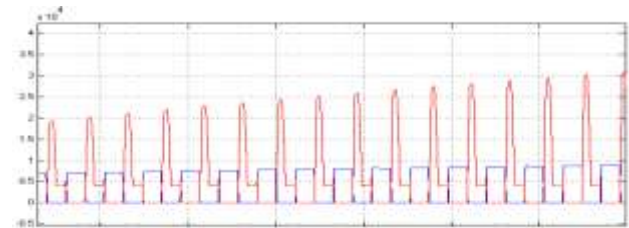


Fig.15. Simulation waveform of the switch voltages (V_{Q1} and V_{Q2}) for 1MW.

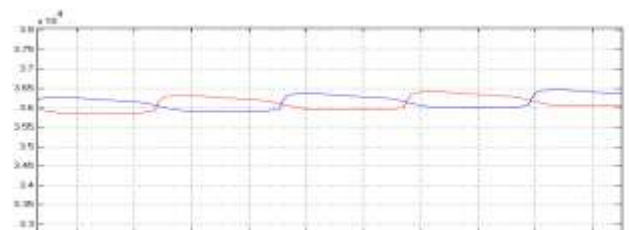


Fig.16. Simulation waveform of the output filter Capacitor Voltages (V_{C1} and V_{C2}) for 1MW.

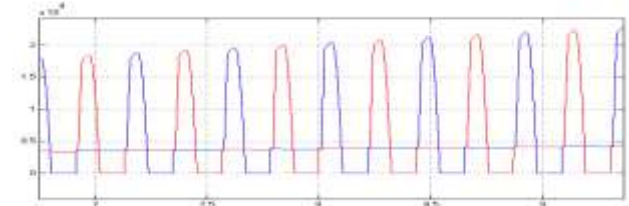


Fig.17. Simulation waveform of the input blocking diodes Voltages (V_{Db1} and V_{Db2}) for 1MW.

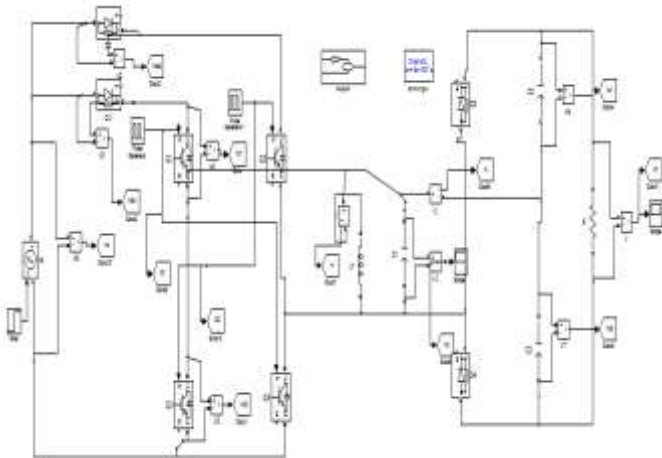


Fig.18. Simulation circuit for input voltage step.

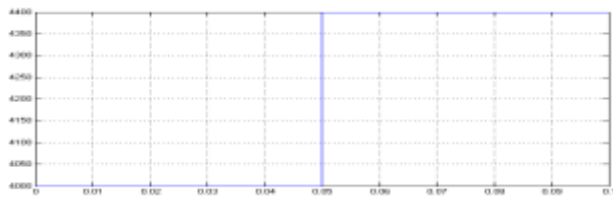


Fig.19. Input Voltage.

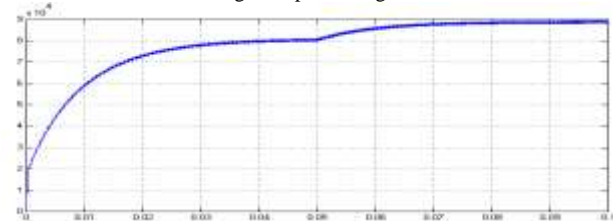


Fig 20. Output Voltage.

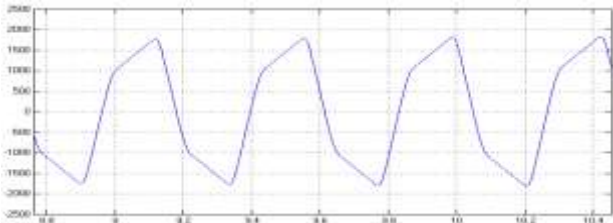


Fig. 21. simulation waveform of resonant inductor current i_{Lr} .

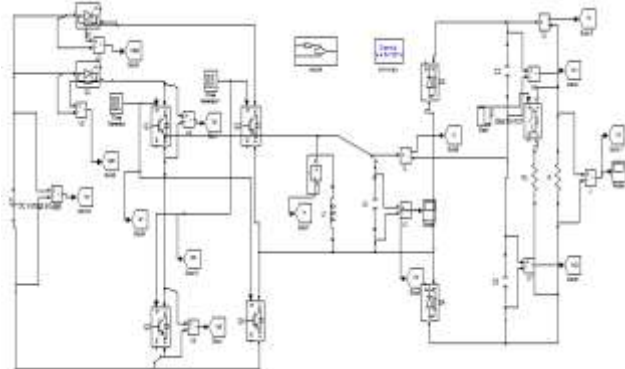


Fig.22. Simulation circuit for step load.

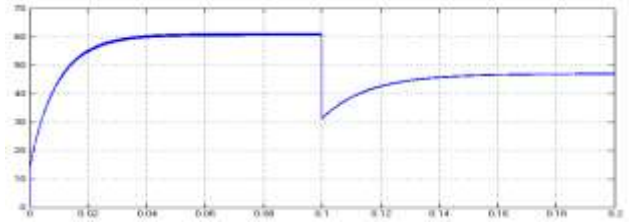


Fig.23. Output Current.

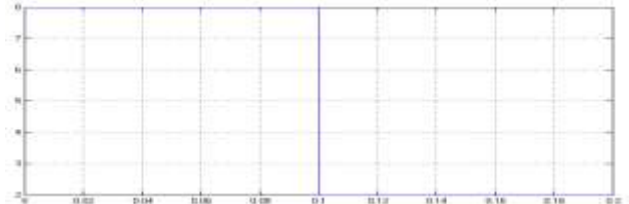


Fig.24. Output Voltage.

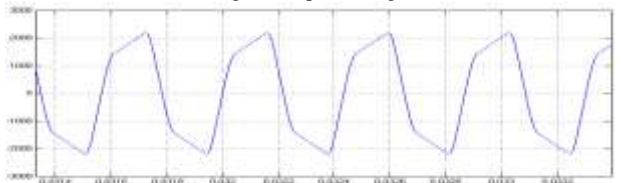


Fig.25. Simulation waveform of resonant inductor current i_{Lr} .

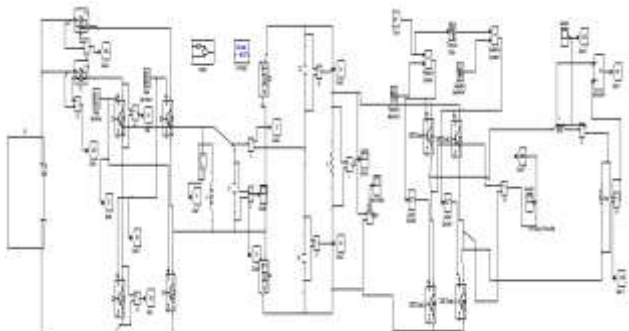


Fig.26. Simulation circuit for grid connected PV cell fed Step-up Resonant Converter.

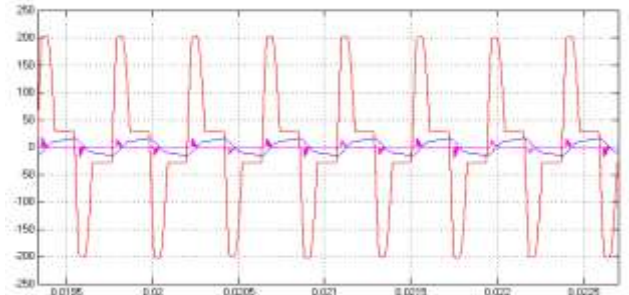


Fig 27 Simulation waveforms of v_{cr} , i_{Lr} , i_c with grid connected system

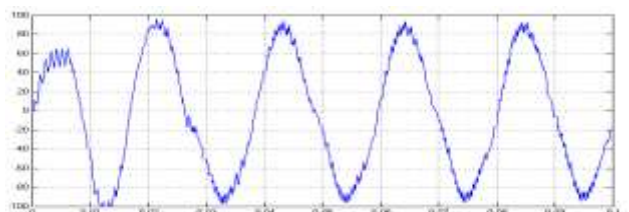


Fig 28 Simulation waveform of step-up converter grid current

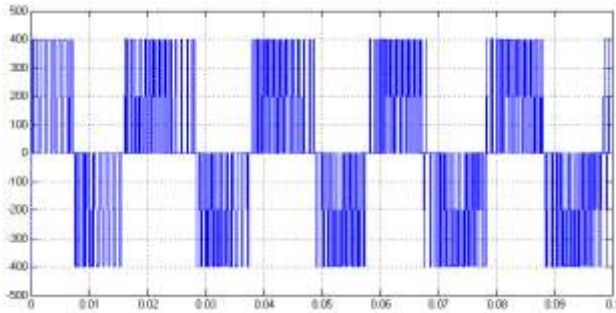


Fig 29 Simulation waveform of step-up converter PWM Output voltage

V. CONCLUSIONS

A step-up resonant converter is proposed in this paper, which can achieve very high step-up voltage gain and it is suitable for high-power high-voltage applications. The converter utilizes the resonant inductor to deliver power by charging from the input and discharging at the output. The resonant capacitor is employed to achieve zero-voltage turn-on and turn-off for the active switches and ZCS for the rectifier diodes. In this paper, the converter was designed to grid connected PV solar energy and was conceived to be a commercially viable high efficiency, and high robustness. Depending of the reactive management in real conditions, the power fluctuation of the PV production is balanced to the power exchanged with the grid or with the batteries. In this context, next and future works will deal with reactive management for real condition operations. The management developed helps integration of PV power into the grid as peak loads are shaved. Depending of the reactive management in real conditions, the power fluctuation of the PV production is balanced to the power exchanged with the grid or with the batteries.

REFERENCES

- [1] Wu Chen, Member, IEEE, Xiaogang Wu, Liangzhong Yao, Senior Member, IEEE, Wei Jiang, Member, IEEE, and Renjie Hu "A Step-up Resonant Converter for Grid-Connected Renewable Energy Sources" IEEE Transactions On Power Electronics, Vol. 30, No. 6, June 2015.
- [2] CIGRE B4-52 Working Group, HVDC Grid Feasibility Study. Melbourne, Vic., Australia: Int. Council Large Electr. Syst., 2011.
- [3] A. S. Abdel-Khalik, A. M. Massoud, A. A. Elserougi, and S. Ahmed, "Optimum power transmission-based droop control design for multi-terminal HVDC of offshore wind farms," IEEE Trans. Power Syst., vol. 28, no. 3, pp. 3401–3409, Aug. 2013.
- [4] F. Deng and Z. Chen, "Design of protective inductors for HVDC transmission line within DC grid offshore wind farms," IEEE Trans. Power Del., vol. 28, no. 1, pp. 75–83, Jan. 2013.
- [5] F. Deng and Z. Chen, "Operation and control of a DC-grid offshore wind farm under DC transmission system faults," IEEE Trans. Power Del., vol. 28, no. 1, pp. 1356–1363, Jul. 2013.
- [6] C. Meyer, "Key components for future offshore DC grids," Ph.D. dissertation, RWTH Aachen Univ., Aachen, Germany, pp. 9–12, 2007.
- [7] W. Chen, A. Huang, S. Lukic, J. Svensson, J. Li, and Z. Wang, "A comparison of medium voltage high power DC/DC converters with high step-up conversion ratio for offshore wind energy systems," in Proc. IEEE Energy Convers. Congr. Expo., 2011, pp. 584–589.
- [8] L. Max, "Design and control of a DC collection grid for a wind farm," Ph.D. dissertation, Chalmers Univ. Technol., Goteborg, Sweden, pp. 15–30, 2009.
- [9] Y. Zhou, D. Macpherson, W. Blewitt, and D. Jovcic, "Comparison of DCDC converter topologies for offshore wind-farm application," in Proc. Int. Conf. Power Electron. Mach. Drives, 2012, pp. 1–6.
- [10] S. Fan, W. Ma, T. C. Lim, and B. W. Williams, "Design and control of a wind energy conversion system based on a resonant dc/dc converter," IET Renew. Power Gener., vol. 7, no. 3, pp. 265–274, 2013.
- [11] F. Deng and Z. Chen, "Control of improved full-bridge three-level DC/DC converter for wind turbines in a DC grid," IEEE Trans. Power Electron., vol. 28, no. 1, pp. 314–324, Jan. 2013.
- [12] C. Meyer, M. Hoing, A. Peterson, and R. W. De Doncker, "Control and design of DC grids for offshore wind farms," IEEE Trans. Ind. Appl., vol. 43, no. 6, pp. 1475–1482, Nov./Dec. 2007.
- [13] C. Meyer and R. W. De Doncker, "Design of a three-phase series resonant converter for offshore DC grids," in Proc. IEEE Ind. Appl. Soc. Conf., 2007, pp. 216–223.